J Nanostruct 8(4): 391-403, Autumn 2018

RESEARCH PAPER

Structural, Magnetic and Dielectric Properties of Dy-doped Co_3O_4 Nanostructures for the Electrochemical Evolution of Oxygen in Alkaline Media

Masumeh Galini, Mehdi Salehi*, Mahdi Behzad

Department of Chemistry, Semnan University, Semnan, Iran

ARTICLE INFO

Article History:
Received 11 June 2018
Accepted 08 September 2018
Published 01 October 2018

Keywords:
Catalytic Activity
Cobalt Oxide
Dielectric Properties
Magnetic Properties
Nano Catalyst

ABSTRACT

In this study, spinel-type cobalt oxide (Co_3O_4) and $Co_{3-x}Dy_xO_4$ (x = 0.04 and 0.05 molar ratio) nanoparticles were synthesized via combustion method at 700 °C. Crystallite nature, phase purity and thermal analysis of the prepared compounds were investigated by PXRD, FT-IR and TGA techniques. Structural analyses were performed by the FullProf program employing profile matching with constant scale factors. The results showed that the patterns had a main cubic structure with space group of Fd3m. The cell parameter data calculated by rietveld analysis showed that the cell parameters were nearly constant. The morphological and structural properties of the obtained materials were examined by FESEM and TEM images. Besides, the magnetic measurements of Co_3O_4 and $Co_{3-x}Dy_xO_4$ nanoparticles were performed by vibration sampling magnetometer (VSM). Coercivity (Hc) and remanent magnetization (Mr) were found to be reduced in Dy^{3+} doped Co_3O_4 while saturation magnetization (Ms) was increased moderately. The effect of dysprosium ion addition was also studied using cyclic voltammetry (CV) for the oxygen evolution reaction in an alkaline environment. The obtained data showed that the presence of Dy^{3+} exhibited a much higher oxygen evolution activity and lower over potential compared to Co_3O_4.

How to cite this article
Galini M, Salehi M, Behzad M. Structural, Magnetic and Dielectric Properties of Dy-doped Co_3O_4 Nanostructures for the Electrochemical Evolution of Oxygen in Alkaline Media. J Nanostruct, 2018; 8(4): 391-403. DOI: 10.22052/JNS.2018.04.009

INTRODUCTION

In recent years, the production of transition metal oxides has attracted the attention of some research groups due to their special properties and envisioned applications in optics, magnetic materials and electronics [1-5]. Among the metal oxides, a great attention has been focused on the synthesis of spinel-type tricobalt tetraoxide (Co_3O_4) which is important in Li-ion rechargeable batteries [6], anti-ferromagnetic p-type semiconductor, heterogeneous effective catalyst in chemical engineering and environmental purification [7-8], magnetic materials [9-10], electrochemical devices [11], etc. In Co_3O_4 (or $CoCo_2O_4$ as AB_2O_4 spinel), the magnetic Co^{2+} ($3d^7$) cations are located in the tetrahedral sites and non-magnetic Co^{3+} ($3d^6$) cations have occupied the octahedral ones. In bulk crystalline form, Co_3O_4 renders antiferromagnetism whereas the nanosized Co_3O_4 shows weak ferromagnetism or superparamagnetism [5]. Until now, several methods such as hydrothermal [12,13], sol–gel [14], chemical spray pyrolysis [15], microemulsion [16], chemical vapor deposition [17], thermal decomposition of cobalt precursors [18] sonochemical route [19], microwave irradiation [20], co-precipitation [21], and mechanochemical processing [22] have been reported for the synthesis of Co_3O_4. But most of these methods require expensive or special instruments and need

* *Corresponding Author Email: msalehi@semnan.ac.ir*

harsh conditions. Combustion method is known as an attractive technique for the synthesis of different oxides, including perovskites, ferrites and zirconia [23-27]. Moreover, the combustion of the corresponding complexes is one of the least expensive and simplest methods for preparing transition metal oxides nanoparticles with high purity [28–31].

In this paper, we present a facile combustion method for the synthesis of spinel-type Co_3O_4 nanoparticles using a classical complex, $[Co(acac)_3]$. So far, several metals have been proposed for the synthesis of doped cobalt oxides. For example, Jang *et al.* [32] prepared Mn-doped Co_3O_4, Jeong et. al. [33] reported α-MnO_2 doped Co_3O_4 and Rahman et. al. [34] reported Cr-doped Co_3O_4. Lanthanide-doped cobalt oxides have also been occasionally reported. Herein we report the synthesis of Dy^{3+}-doped Co_3O_4 nanostructure by combustion of $[Co(acac)_3]$. The morphology, structure, thermal behavior and magnetic properties of the as prepared Co_3O_4 and Dy^{3+}-doped Co_3O_4 nanostructures were investigated by SEM, TEM, XRD, FT-IR spectra, cyclic voltammetry (CV), TGA and VSM.

EXPERIMENTAL

Materials and Characterization techniques

All the chemicals and solvents were of analytical grade and were used without further purifications. Fourier transform infrared (FT-IR) spectrum were measured by a FT-IR SHIMADZU spectrophotometer, with KBr pellet technique in the wavelength range from 4000-400 cm-1 to measure the structural components. The crystallographic information and phase purity of the samples was obtained with the X-ray powder diffraction (XRD) using Bruker D8000 Germany in a scanning range of 2θ = 10–90°. The morphological, structural and particle size distribution of the nanostructures of Co_3O_4 were carried by the Hitachi FESEM model S-4160 field emission scanning electron microscope (FESEM) and a transmission electron microscopy (TEM, Philips-CM300). Thermal analysis (TGA) curve were recorded with a STA PT 1600- Linseis(Germany) using a heating rate of 5 ºC.min^{-1} in air atmosphere. Also, magnetic measurements were carried out with a vibrating sampling magnetometer (VSM, Model 7400- LakeShore). All electrochemical tests were done by a Metrohm instrument, Model 797 VA processor, or an Autolab potentiostat-galvanostat, Model PGSTAT302. A platinum wire as a counter electrode, an Ag/AgCl (3.0 mol L^{-1} KCl) reference electrode and a modified or unmodified glassy carbon electrode (GCE) as a working electrode were placed in a cell containing electrolyte, and then it was used as a conventional three-electrode system for all the electrochemical experiments. All the potentials reported in this work are vs. Ag/AgCl (3.0 mol L^{-1} KCl).

Preparation $[Co(acac)_3]$ complex as a precursor

The complex was synthesized relevant to the general synthetic method in the literature. In a typical synthesis procedure, 0.38 g (0.0015mmol) of $Co(CH_3COO)_2.4H_2O$ was dissolved into 5 mL distilled water and was heated to about 90°C using a hot water bath with ongoing stirring, then 3 mL of acetylacetone was added. While maintaining the reaction temperature around 90°C, 4.5 mL of 35% H_2O_2 was added drop-wise, using a dropping pipette during 20 min. The reaction flask was covered by a watch glass during the hydrogen peroxide addition. Stirring was retained throughout the addition and then for a further 15 minutes. After this step, the reaction flask was cooled in an ice- water bath for 20 minutes. Dark green precipitate was filtered under vacuum, washed with distilled water, vacuum dried for10 minutes and then dried in the oven at 100 °C. Yield: 75%. FT-IR: v_{max} cm^{-1} (KBr): 1565 (w, C-H), 1573 (C=O), 1512 (C=C).

Preparation of Co_3O_4 nanoparticles

An appropriate amount of the $[Co(acac)_3]$ complex powder (2g) as the precursor for the synthesis of Co_3O_4 (S_1) was transferred into a crucible. To prevent the possibility of dispersion, it was turned gel-like with a small amount of distilled water. The crucible containing the complex was heated at 700 °C for 8h. The black powder

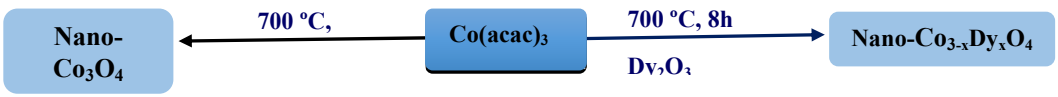

Fig. 1. Synthetic protocol of Co_3O_4 and $Co_{3-x}Dy_xO_4$ nanoparticles.

obtained from the calcination was collected for characterization. Yield: 85%. FT-IR: v_{max} cm^{-1} (KBr): : 665 (Co-O), 576 (Co-O), 1512 (C=C).

Preparation of $Co_{3-x}Dy_xO_4$ nanoparticles

Proper molar amounts of $[Co(acac)_3]$ (1.96, 1.95) and Dy_2O_3 (0.04 (S_2) and 0.05 (S_3), respectively), were added to a crucible. It was then heated at 700 °C for 8h. The obtained sample powder ($Co_{3-x}Dy_xO_4$) was collected for characterization and for comparison with the pure cobalt oxide.

Preparation of the electrodes

The GCE was polished mechanically with 5 µm alumina slurry on a polishing cloth. Afterwards, the electrode was washed ultrasonically in a mixture of ethanol/distilled water solution (1:1 V/V) for 10 min and dried in the room temperature.

To deposit Co_3O_4 and $Co_{1.96}Dy_{0.04}O_3$ on the electrode, a relative stable suspension were obtained by ultrasonically dispersing of the synthesized powders (0.10 mg) in 10 mL distilled water. Then, 5.0 µL of the suspension was dropped on the electrode and allowed to dry in the air at room temperature. Finally, 5 µL of 1% wt. Nafion solution was dropped onto the electrode to increase the adhesion of the coatings to the surface.The Co_3O_4/GCE and $Co_{1.96}Dy_{0.04}O_3$/ GCE, were obtained using the above mentioned procedure.-

RESULTS AND DISCUSSION

X-ray diffraction studies

Fig. 2. shows the XRD pattern of $[Co(acac)_3]$ complex. All diffraction peaks in this XRD pattern matched very good with those reported in the literature for the pure $[Co(acac)_3]$ complex with JCPDS Card no. 24-1627. XRD technique was used to check the crystallinity and phase purity of the as-prepared Co_3O_4 (Fig. 3 (a). Our analysis revealed that all diffraction peaks were sharp and slender, which insinuate the excellent degree of crystallinity. The XRD patterns of the sample indicated obvious diffraction peaks corresponding to 2θ = 19.01º, 31.28º, 36.87º, 38.59º, 44.82º, 55.68º, 59.4º and 65.25º which were assigned to the (111), (220), (311), (222), (400), (422), (511) and (440) crystalline planes, respectively. Also, Structural analysis was done by the *FullProf* program by employing profile matching with constant scale factor. Red bars are observed intensities in which obtained from the diffraction data. Black ones are calculated data. Blue one is the difference: Yobs-Ycalc. The bars below indicate the Bragg reflections. Since we have two lines of bars, it means there are two phases. The upper one is corresponded to Co_3O_4 and the below one is due to Dy_2O_3. For comparison, we included the impurity phase in both S_2 and S_3 to confirm that the impurity phase is apparent in S_3. The obtained data confirmed the synthesis of Face Centered Cubic phase spinel Co_3O_4 crystalline structure with lattice parameters of about a = b = c = 8.08 Å according to the JCPDS Card no. 43-1003 and space group Fd3m [38]. This result confirmed the complete decomposition of precursor $[Co(acac)_3]$ into Co_3O_4 crystal phase at 700 ºC. Preliminary structural investigation of all doped samples in $Co_{3-x}Dy_xO_4$ were determined by analyzing the X-ray diffraction patterns. Fig. 3b shows the XRD patterns of $Co_{3-x}Dy_xO_4$ in different molar ratio (x = 0.04 and 0.05) indicates that the positions of characteristic

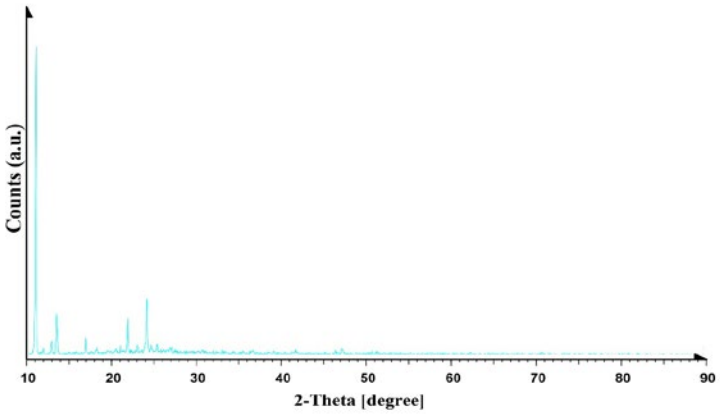

Fig. 2. XRD pattern of the $[Co(acac)_3]$ precursor.

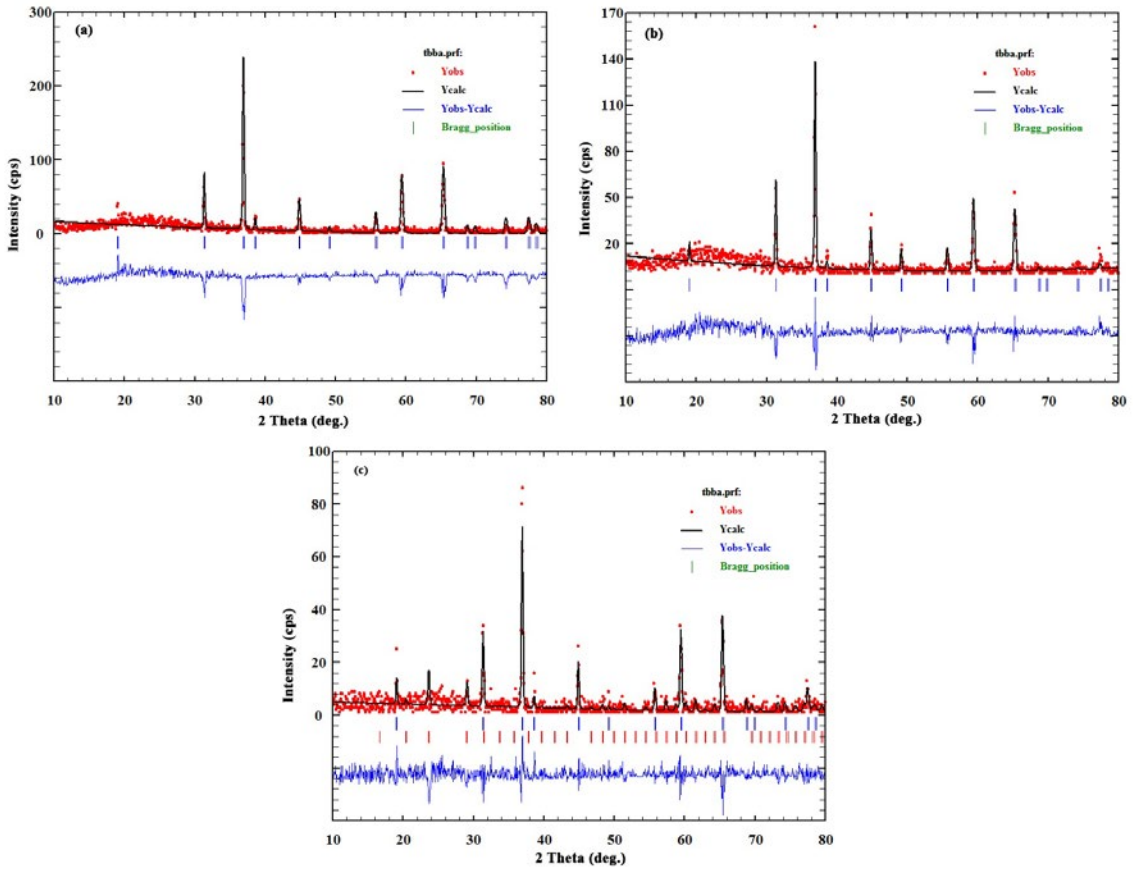

Fig. 3. XRD patterns of Co_3O_4 pure (a) and Dy^{3+} doped Co_3O_4 in (b= 0.04 and c= 0.05 mmol of dopant) obtained from combustion method at 700 °C for 8 h.

Table 1. Scherrer data information for pure $Co_{3-x}Dy_xO_4$ nanomaterials obtained after 8 h at 700 °C in x = 0.0, 0.04 and 0.05 mmol.

	S_1	S_2	S_3
2 θ	36.8664	36.8903	36.9121
FWHM	0.23554	0.23334	0.23251
$B_{1/2}$	0.00410	0.00407	0.004056
Cos (θ)	0.9487	0.9486	0.9486
D (nm)	36	36	36
Cell parameter(Å)	8.079486	8.084304	8.071710
χ^2	2.66	1.86	1.37

peaks for the doped sample from x= 0.04 is consistent with those of undoped cobalt oxide in Fig. 3(a). This indicates that dysprosium ions have been well accommodated into cobalt lattice sites without grable crystal symmetry. According to Fig. 3c, increasing the amount of dopant Dy^{3+} ions to x= 0.05 shows diffraction lines (red bars) at 2θ ≈ 28.98°, 43.28° which could be assigned to the (222) and (134) crystalline planes of excess Dy_2O_3. Only a small fraction of the total amount of Dy^{3+} ions goes into the cobalt sites and additional amount may be on the grain boundaries of the nanocrystals or stay on the surface [40]. Therefore, the maximum amount of doped ion is 0.05 mmol.

Table 1 shows the average particle size of the nanostructures calculated using the Scherrer's equation [39]:

$$D = 0.9\lambda / \beta \cos\theta \qquad (1)$$

Where D, λ, θ and β are the average crystalline size, the X-ray wavelength of Cu K_α, the Bragg's diffraction angle and the full width at half maximum (FWHM) of the diffraction peak respectively.

Besides, Table 1. shows cell volume and reduced

average crystallite sizes of $Co_{3-x}Dy_xO_4$ in different molar ratios (x = 0.04 and 0.05). Table 1. indicates that the added Dy^{3+} has prevented the increasing the crystallite size. The observed very little decreasing the cell volume and very little increasing average crystallite size is due to the difference in the ionic radius of dysprosium and cobalt ions (ionic radius of Dy^{3+} = 0.91 A°, Co^{2+} = 0.65 A° and Co^{3+} = 0.61 A°) [41]. The χ^2 values obtained from the rietveld analyses show the goodness of the analysis.

FTIR spectra

Fig. 4. shows the FT-IR spectra of the $[Co(acac)_3]$ complex and its calcination product at 700 °C. The spectrum of $[Co(acac)_3]$ shows the characteristic absorption band of the resonant C=O vibration at 1573 cm^{-1}. For the calcined sample (Co_3O_4), the obtained results matched well with the spinel-type Co_3O_4 structure. Inspection of this spectrum revealed the presence of only two characteristic bands of the cobalt oxide at 576 cm^{-1} (v_1) and 665 cm^{-1} (v_2) which were due to the M-O vibrations, confirming complete decomposition of the $[Co(acac)_3]$ complex to the cobalt oxide and the formation of spinel Co_3O_4 [12,35-36]. The v_1 band is characteristic of Co^{3+} vibration in the octahedral site formed by the oxide ions and the v_2 band is assigned to the Co^{2+} vibrations in the tetrahedral sites, in the spinel lattice [37].

Field emission scanning electron microscope (FESEM)

Fig. 5. shows the FESEM images of spinel Co_3O_4 prepared via the combustion of $[Co(acac)_3]$ complex without using fuel. As could be seen, the prepared Co_3O_4 nanoparticles exhibited a spherical morphology with holes randomly distributed among them and the pore sizes of about 50-100 nm with high density.

Figs. 6-7 display the FESEM images of the Dy^{3+}-doped Co_3O_4 (x = 0.04 and 0.05 mmol, respectively). As could be seen from Fig. 6, the pores have multigonal structure and pore sizes are about 50-150 nm. The particles of the porouses are homogeneous, so porouses became homogeneous too. According to Fig. 7, by doping Dy^{3+} in Co_3O_4 structure, porouse layer particles and some particles have been seen so that porouses in Fig. 7a and b have two small sizes with a medium size about 30-50 nm and large size with a medium size about 200 nm.

Transmission electron microscopy (TEM)

The physical nature and exact size of the particles of the Co_3O_4 were determined by TEM. Fig. 8 shows TEM images of the as prepared Co_3O_4 nanoparticles with fusiform-like morphology and multigonal particles. Moreover, the particles of tricobalt tetraoxide have homogeneous and uniform distribution in the powder sample. For obtaining the exact size of the particles, manual analysis has been done which is shown in Fig. 8. In this plot, the particle size is about 100 nm. Fig. 10 shows TEM images of the S_2. As is seen in Fig. 11, the particles sizes are in the range of 14 nm to 18 nm. According to the TEM image, it could be recognized that the used preparation method is

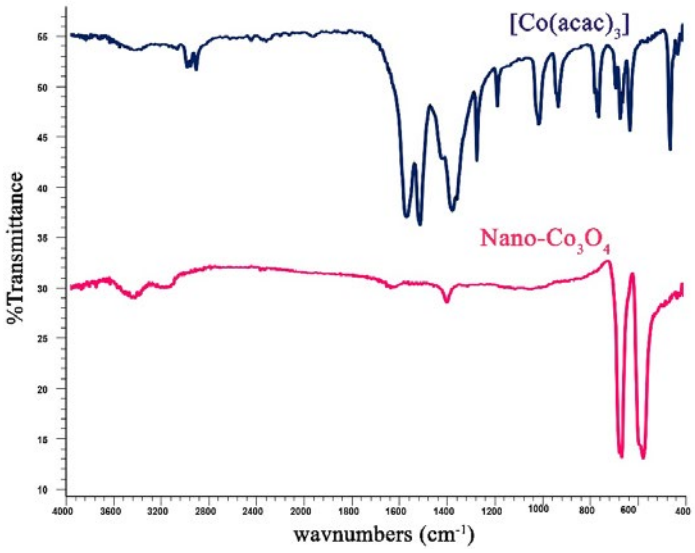

Fig. 4. FT-IR spectrum of $[Co(acac)_3]$ complex and Co_3O_4 nanoparticles.

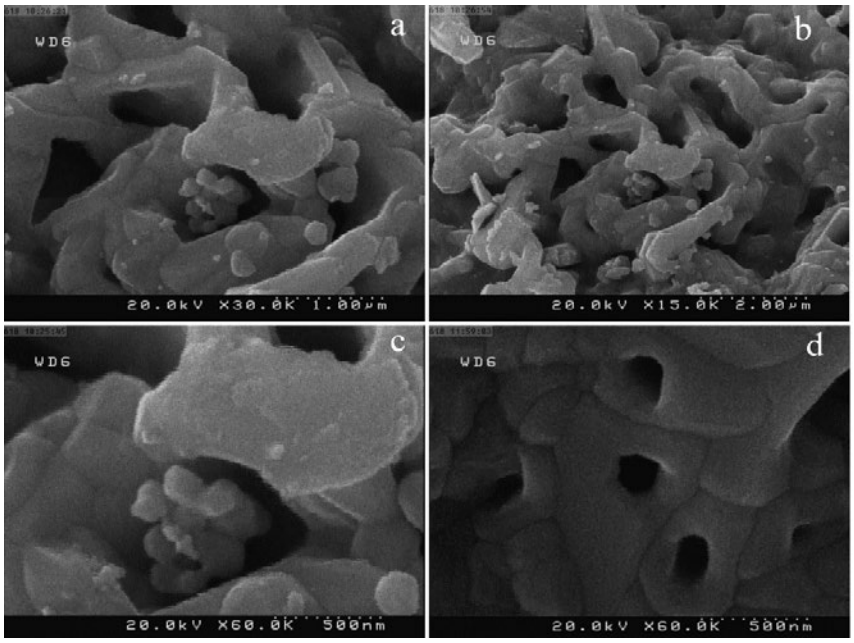

Fig. 5. FESEM images of Co_3O_4.

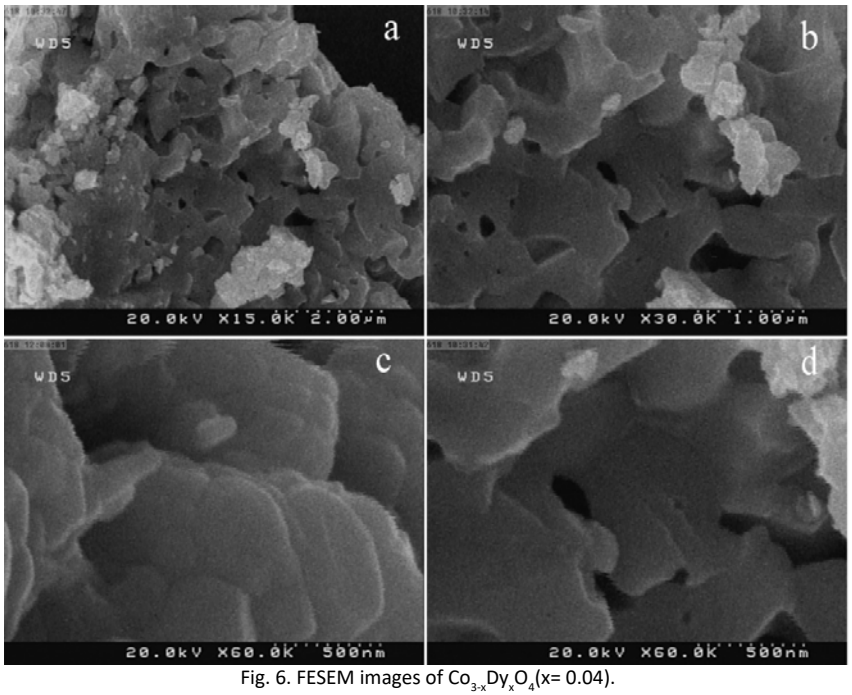

Fig. 6. FESEM images of $Co_{3-x}Dy_xO_4$(x= 0.04).

suitable to obtain the nanoparticles of $Co_{3-x}Dy_xO_4$. Low Dy^{3+} amount is recommended in Co_3O_4 synthesis to avoid agglomeration of the particles, higher homogeneity and to obtain powder with smaller size in comparison with undoped sample.

Elemental map analysis (Fig. 12) was used for investigation of elemental distributions in synthesized $Co_{2.96}Dy_{0.04}O_4$. It can be seen from fig. 9 that Dy, Co and O in $Co_{2.96}Dy_{0.04}O_4$ are uniformly distributed in this work. Also, Fig. 13 shows the EDS elemental analysis for $Co_{2.96}Dy_{0.04}O_4$. Results show the presence of 54.99 at.% O, 1.87 at.% Dy, 3.23 at C and 39.91 at.% Co, for the $Co_{2.96}Dy_{0.04}O_4$ that confirm MAP analysis investigation. Presence of C

is relative to acetylacetone ligand after burning.

Thermal analysis

The TG thermogram of nano-Co_3O_4 with heating rate of 5 $^oC.min^{-1}$ in air atmosphere as carrier gas is shown in Fig. 14. The TG curve shows two weight loss (WL) steps from ambient temperature till 1000 ºC. In the first weight loss step, the TGA showed a gradual weight loss (8%) up to around 160 ºC with the temperature rise which corresponds to loss of structural water [42]. The seconds weight loss step occurs at the 890-920 ºC temperature range with 10% weight loss, which is due to the decomposition of Co_3O_4 into CoO and O_2 according to the following equilibrium [43]:

$$Co_3O_4 \rightleftharpoons CoO+1/2O_2$$

Electrochemical impedance spectroscopy

The electrical conductivity effects of the synthesized nanoparticles were investigated using EIS. Electron transfer resistance, R_{ct} is an important factor for this goal. The semicircle portion at higher frequencies corresponded to the electron

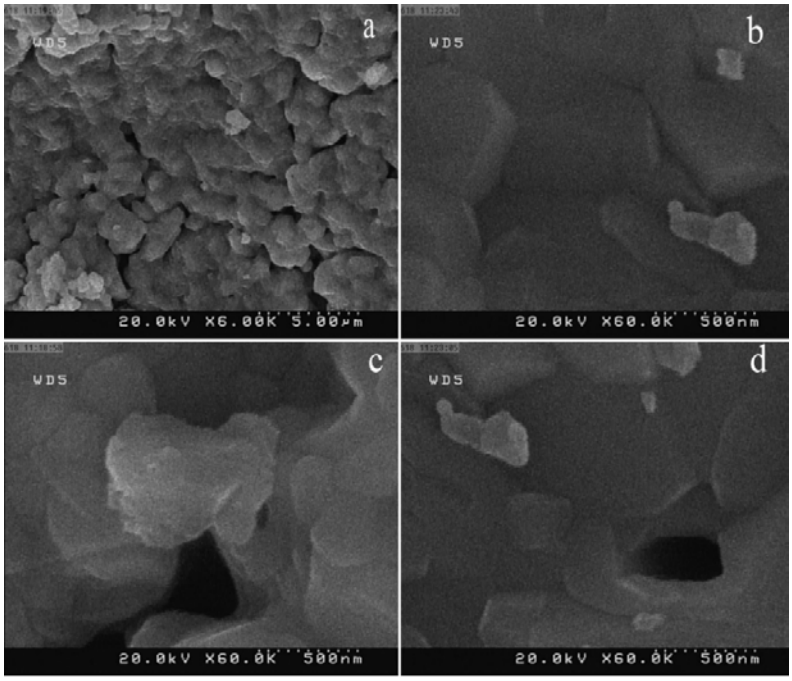

Fig. 7. FESEM images of $Co_{3-x}Dy_xO_4$(x= 0.05).

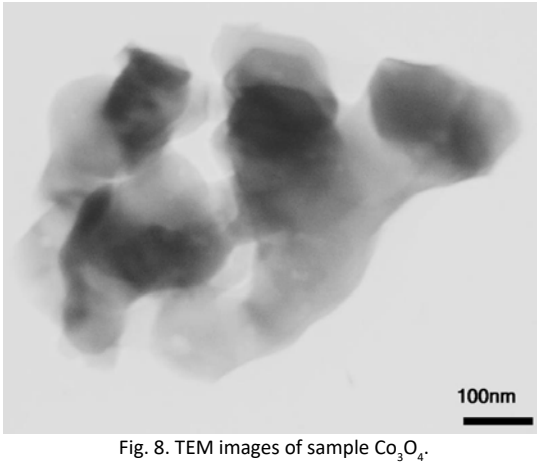

Fig. 8. TEM images of sample Co_3O_4.

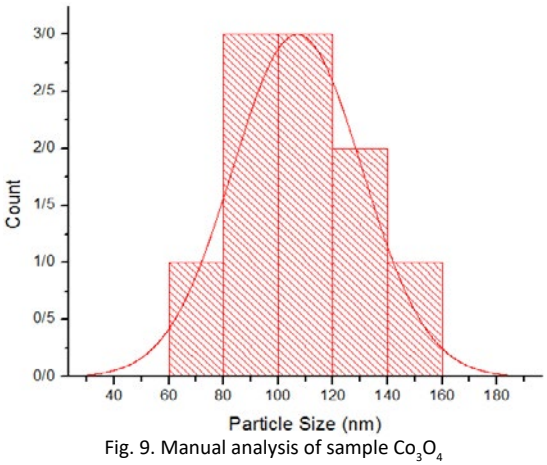

Fig. 9. Manual analysis of sample Co_3O_4

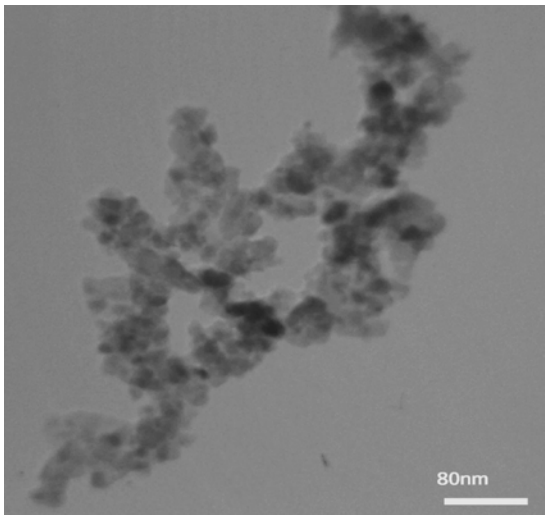

Fig. 10. TEM images of sample $Co_{3-x}Dy_xO_4$ (x= 0.04).

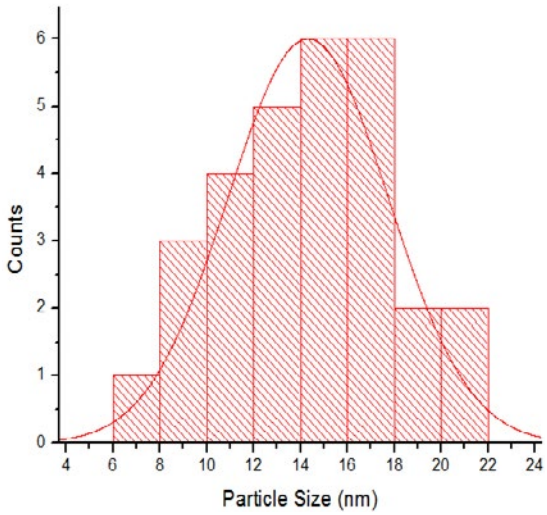

Fig. 11. Manual analysis of sample $Co_{3-x}Dy_xO_4$ (x= 0.04).

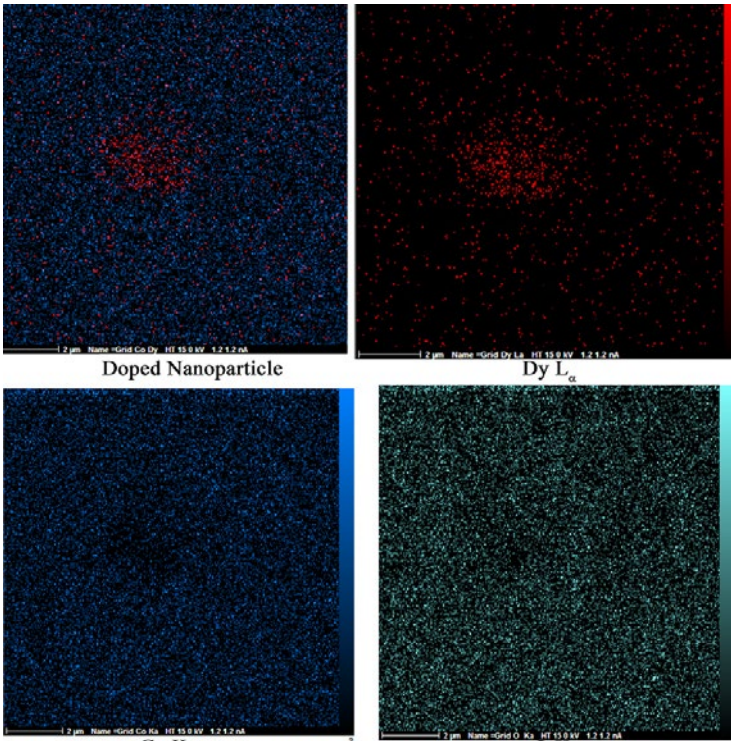

Fig. 12. Maps of Co, Dy and O distributions in sample $Co_{1.96}Dy_{0.04}O_3$.

transfer limited process for a conductive surface or electroactive compound. Fig. 15 shows the impedance plots for (a) GCE, (b) Co_3O_4/GCE, and (c) $Co_{3-x}Dy_xO_4$/GCE in 1.0 mM $[Fe(CN)_6]^{3-/4-}$ (1:1) solution in 0.1 M KCl. It is evident from the EIS data, at a surface of GCE modified with Co_3O_4, the electron transfer resistance was at its minimum value that is relative to the high conductivity effect of Co_3O_4 at the surface of electrode. Also, the R_{ct} for GCE modified with $Co_{1.96}Dy_{0.04}O_3$ is high compared to Co_3O_4 that shows doping of Dy^{3+} reduces electrical conductivity of Co_3O_4.

Magnetic measurements

The magnetic characterization of the prepared pure and doped Co_3O_4 was examined using

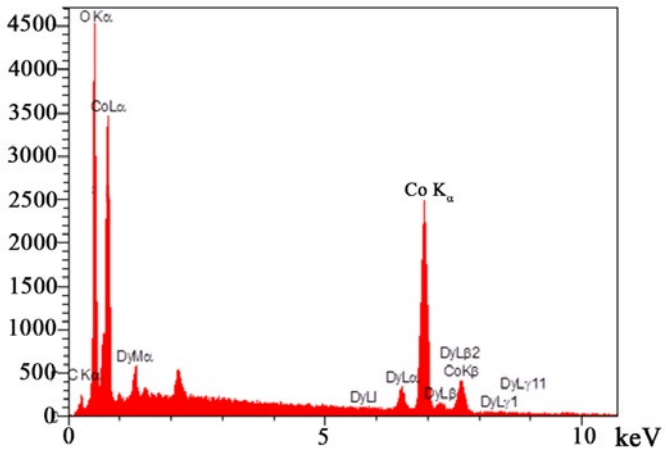

Fig. 13. EDS analysis of the powders $Co_{1.96}Dy_{0.04}O_3$.

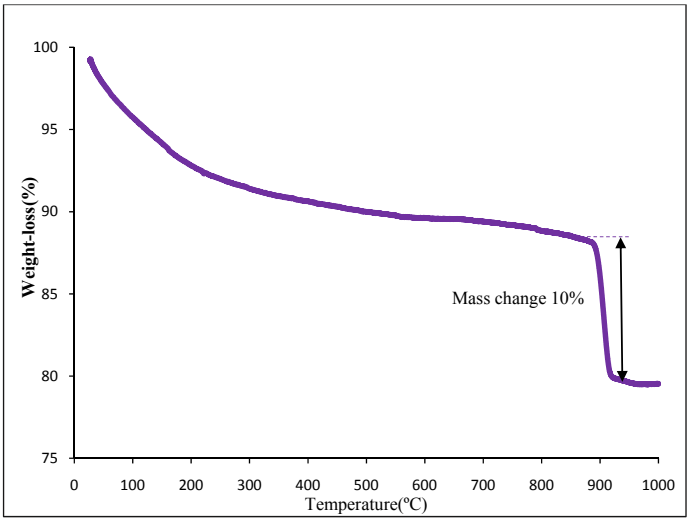

Fig. 14. TG thermograms of Co_3O_4 nanoparticles in air atmosphere in the temperature range from 25–1000 °C and heating rate of 5 °C min^{-1}.

vibration sampling magnetometer (VSM). The magnetic behavior of the samples in the M-H (M- magnetization (memu/g) and H- magnetic field (Gouss)) curve are shown in Fig. 16(a-b), respectively. The Co_3O_4 nanoparticles and $Co_{3-x}Dy_xO_4$ showed a weak ferromagnetic nature in which, a tiny hysteresis loop can be seen for pure Co_3O_4. In general, bulk Co_3O_4 has normal spinel structure with antiferromagnetic exchange between ions accupying the tetrahedral A (high spin Co^{2+}) sites and the octahedral B (low spin Co^{3+}) sites [44]. It is known that for bulk antiferromagnetic materials, zero net magnetization is due to the complete compensation of sublattice magnetizations. Hence, the change from an antiferromagnetic behavior for bulk Co_3O_4 to a weak ferromagnetic behavior for Co_3O_4 nanoparticles can be attributed to the uncompensated surface spins and/or finite size effects of the tericobalt tetraoxide nanoparticles [45-47]. For the weak ferromagnetic behavior of the antiferromagnetic nanostructured material, different models have been proposed, such as Co_3O_4 mesoporous [48], CoO thin layers [49], Co_3O_4 nanoparticles [9,10, 50-53] and ferromagnetic behavior in cobalt oxide nanoparticles based on finite size effect [54]. The Dy^{3+} ions substituted cobalt ions in both positions and have changed the magnetic interactions between the two sites; this change can cause magnetic parameters change compared to the pure Co_3O_4. With doping the dysprosium oxide, remanent magnetization (Mr) and coercive force (Hc) has been reduced, which

is shown in Table 2. Also, the hysteresis loop is not observed in doped sample.

Catalytic activity for oxygen evolution

Oxygen evolution reaction (OER) is one of the most important processes in various electrochemical devices. Spinal-type Co_3O_4, an inexpensive material, has shown high activity and long term performance for OER in alkaline electrolyte. Therefore, many studies have been

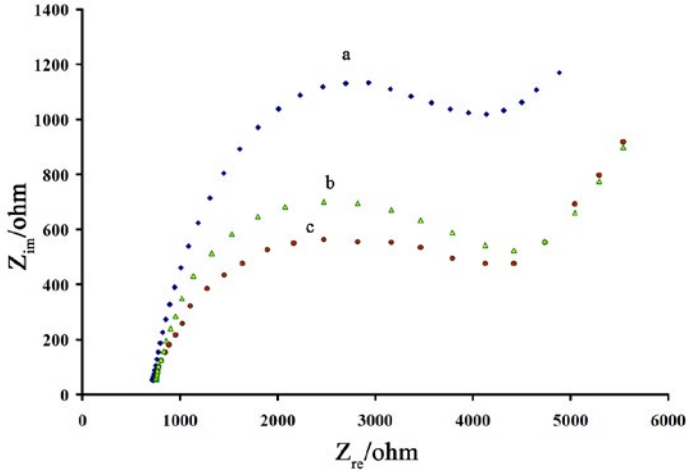

Fig. 15. Nyquist diagrams of 1 mM $K_4[Fe(CN)_6]$ in the presence of 0.1 M KCl. (a) bare carbon paste electrode, (b) carbon paste electrode with $Co_{1.96}Dy_{0.04}O_3$, and (c) carbon paste electrode with Fe_2O_3nanoparticle

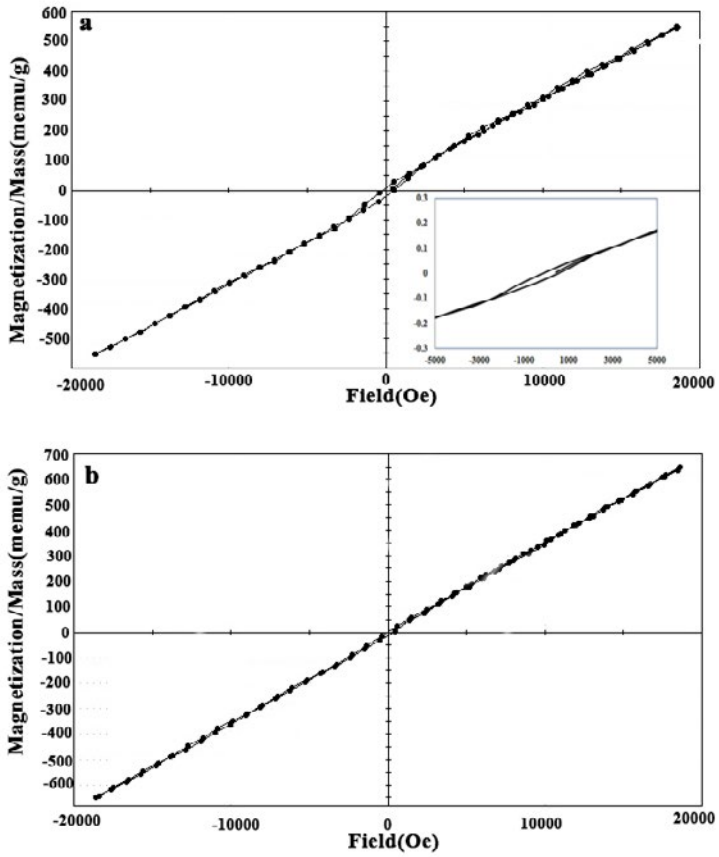

Fig. 16. Magnetization measurements at room temperature of $Co_{3-x}Dy_xO_4$ nanostructure in x= 0.0 and 0.05 of Dy^{3+}. The inset shows the magnification of the hysteresis loop at $Co_{3-x}Dy_xO_4$ (x = 0.0).

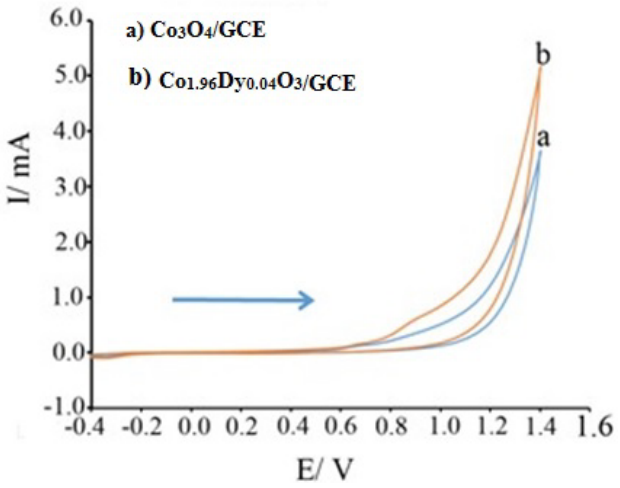

Fig. 17. CV curves for (a) Co3O4/GCE, and (b $Co_{1.96}Dy_{0.04}O_3$ /GCE in 0.1 mol L^{-1} KOH with a sweep rate of 0.05 Vs^{-1}.

Table 2. Remanent magnetization (Mr), saturation magnetization (Ms) and coercive force (Hc) for $Co_{3-x}Dy_xO_4$ in x= 0.0 and 0.04 of Dy^{3+}.

X (molar ratio)	-Hc(G)	Hc(G)	-Mr (emu/g)	Mr(emu/g)	-Ms(emu/g)	Ms(emu/g)	Average particle size (nm)
0.0	145.90	537.83	20.73	5.68	0.5534	0.5534	37.89
2.5	46.51	348.55	12.78	1.89	0.6493	0.6493	36.89

devoted to the improvement of the composition and structure of Co_3O_4 to increase of OER efficiency. The doping of various metals in Co_3O_4 structure is one way that is employed to increase the performance of Co_3O_4.

The effect of dysprosium doping on the electrocatalytic activity of Co_3O_4 was studied using cyclic voltammetry (CV) for the OER in alkaline media. Fig. 17 shows that the presence of dysprosium increases the current of the oxygen evolution.

At a fixed potential of 1.2 V, current value for $Co_{2.96}Dy_{0.04}O_4$/GCE is 1.79 mA, which is about 1.5 times higher than 1.22 mA for Co_3O_4/GCE. Moreover, it is found that at a fixed current of 1.50 mA, the potential is 1.16 V for $Co_{2.96}Dy_{0.04}O_4$/GCE and 1.24 V for Co_3O_4/GCE, i.e. the overpotential is improved 0.08 V by doping dysprosium. The performance improvement of OER by dysprosium may be due to an increase in electrical conductivity, as evidenced using EIS in section 3.6.

CONCLUSIONS

In this paper, nanosized Co_3O_4 and Dy^{3+}-doped Co_3O_4 nanoparticles were successfully prepared by the combustion of [Co(acac)$_3$] complex at 700 ºC. FT-IR and X-ray diffraction (XRD) investigates confirmed the Co_3O_4 and $Co_{3-x}Dy_xO_4$ formation and showed the purity of the compounds. TG curve showed a reasonable thermal behavior of cobalt oxide. Surface morphology and particle size distribution of the synthesized materials investigated by FESEM and TEM images, also confirmed dysprosium role in better distribution of nanoparticles and in particle growth reduction. From this images, the spherical morphology was observed with holes randomly distributed among them in the Co_3O_4, while in the $Co_{3-x}Dy_xO_4$ the pores have multigonal structure. Porouse layer particles and doping of Dy^{3+} ions promotes improved morphology of $Co_{3-x}Dy_xO_4$ nanostructures with higher uniformity compared to pure Co_3O_4. Weak ferromagnetic behavior was observed in the compounds using the VSM measurements. A small hysteresis loop was observed for pure Co_3O_4, while Dy^{3+} ions replacing cobalt lattice site, caused magnetic parameters change compared to the pure Co_3O_4 and the hysteresis loop was not observed in doped sample. Finally, we studied the effect of dysprosium additive on charge transfer resistance and oxygen evolution reactions. The results indicated that dysprosium increased the Co_3O_4 conductivity and its catalytic activity towards OER.

ACKNOWLEDGEMENTS

We thank Semnan University for supporting this study.

CONFLICT OF INTEREST

The authors declare that there are no conflicts of interest regarding the publication of this manuscript.

REFERENCES

1. Zheng Z, Huang L, Zhou Y, Hu X, Ni X. Large-scale synthesis of mesoporous CoO-doped NiO hexagonal nanoplatelets with improved electrochemical performance. Solid State Sciences. 2009;11(8):1439-43.
2. Lee JW, Ahn T, Kim JH, Ko JM, Kim J-D. Nanosheets based mesoporous NiO microspherical structures via facile and template-free method for high performance supercapacitors. Electrochimica Acta. 2011;56(13):4849-57.
3. Chen H, Chu PK, He J, Hu T, Yang M. Porous magnetic manganese oxide nanostructures: Synthesis and their application in water treatment. Journal of Colloid and Interface Science. 2011;359(1):68-74.
4. Al-Gaashani R, Radiman S, Tabet N, Razak Daud A. Synthesis and optical properties of CuO nanostructures obtained via a novel thermal decomposition method. Journal of Alloys and Compounds. 2011;509(35):8761-9.
5. Ozkaya T, Baykal A, Toprak MS, KoseoÄŸlu Y, DurmuÅŸ Z. Reflux synthesis of Co3O4 nanoparticles and its magnetic characterization. Journal of Magnetism and Magnetic Materials. 2009;321(14):2145-9.
6. Poizot P, Laruelle S, Grugeon S, Dupont L, Tarascon JM. Nano-sized transition-metal oxides as negative-electrode materials for lithium-ion batteries. Nature. 2000;407(6803):496-9.
7. Kim H, Won Park D, Chul Woo H, Shik Chung J. Reduction of SO2 by CO to elemental sulfur over Co3O4-TiO2 catalysts. Applied Catalysis B: Environmental. 1998;19(3-4):233-43.
8. Å vegl F, Orel B, Bukovec P, Kalcher K, Hutchins MG. Spectroelectrochemical and structural properties of electrochromic Co(Al) -oxide and Co(Al,Si) -oxide films prepared by the sol-gel route. Journal of Electroanalytical Chemistry. 1996;418(1-2):53-66.
9. Nethravathi C, Sen S, Ravishankar N, Rajamathi M, Pietzonka C, Harbrecht B. Ferrimagnetic Nanogranular Co3O4 Through Solvothermal Decomposition of Colloidally Dispersed Monolayers of Î±-Cobalt Hydroxide. ChemInform. 2005;36(38).
10. Ichiyanagi Y, Yamada S. The size-dependent magnetic properties of Co3O4 nanoparticles. Polyhedron. 2005;24(16-17):2813-6.
11. Zhao Y, Wan X, Xu X, Cao G, Yang J. Comparison of Via Electromigration with Self-Ionized Plasma and MOCVD Methods for Barrier Metal Deposition. Journal of The Electrochemical Society. 2005;152(11):G831.
12. Chen Y, Zhang Y, Fu S. Synthesis and characterization of Co3O4 hollow spheres. Materials Letters. 2007;61(3):701-5.
13. Li L, Chu Y, Liu Y, Song J, Wang D, Du X. A facile hydrothermal route to synthesize novel Co3O4 nanoplates. Materials Letters. 2008;62(10-11):1507-10.
14. El Baydi M, Poillerat G, Rehspringer J-L, Gautier JL, Koenig J-F, Chartier P. A Sol-Gel Route for the Preparation of Co3O4 Catalyst for Oxygen Electrocatalysis in Alkaline Medium. Journal of Solid State Chemistry. 1994;109(2):281-8.
15. Kim DY, Ju SH, Koo HY, Hong SK, Kang YC. Synthesis of nanosized Co3O4 particles by spray pyrolysis. Journal of Alloys and Compounds. 2006;417(1-2):254-8.
16. Wang RM, Liu CM, Zhang HZ, Chen CP, Guo L, Xu HB, et al. Porous nanotubes of Co3O4: Synthesis, characterization, and magnetic properties. Applied Physics Letters. 2004;85(11):2080-2.
17. Xuan Y, Liu R, Jia YQ. Synthesis of a new series of compounds RE2Co2/3Nb4/3O7 and stability field diagram of RE2B2/3'B4/3"O7 pyrochlore compounds. Mater Chem Phys. 1998;53(3):256-261.
18. Salavati-Niasari M, Mohandes F, Davar F. Preparation of PbO nanocrystals via decomposition of lead oxalate. Polyhedron. 2009;28(11):2263-7.
19. Kumar RV, Diamant Y, Gedanken A. Sonochemical Synthesis and Characterization of Nanometer-Size Transition Metal Oxides from Metal Acetates. Chemistry of Materials. 2000;12(8):2301-5.
20. Bhatt AS, Bhat DK, Tai C-w, Santosh MS. Microwave-assisted synthesis and magnetic studies of cobalt oxide nanoparticles. Materials Chemistry and Physics. 2011;125(3):347-50.
21. Lai T-L, Lai Y-L, Lee C-C, Shu Y-Y, Wang C-B. Microwave-assisted rapid fabrication of Co3O4 nanorods and application to the degradation of phenol. Catalysis Today. 2008;131(1-4):105-10.
22. Wang X, Chen X, Gao L, Zheng H, Zhang Z, Qian Y. One-Dimensional Arrays of Co3O4Nanoparticles:Â Synthesis, Characterization, and Optical and Electrochemical Properties. The Journal of Physical Chemistry B. 2004;108(42):16401-4.
23. Patil KC, Aruna ST, Mimani T. Combustion synthesis: an update. Current Opinion in Solid State and Materials Science. 2002;6(6):507-12.
24. Dong XC, Xu H, Wang XW, Huang YX, Chan-Park MB, Zhang H, Wang LH, Huang W, Chen P. 3D graphene–cobalt oxide electrode for high-performance supercapacitor and enzymeless glucose detection. ACS nano. 2012;6(4):3206-13.
25. Mukasyan AS, Costello C, Sherlock KP, Lafarga D, Varma A. Perovskite membranes by aqueous combustion synthesis: synthesis and properties. Separation and Purification Technology. 2001;25(1-3):117-26.
26. Rao GR, Sahu HR, Mishra BG. Surface and catalytic properties of Cu–Ce–O composite oxides prepared by combustion method. Colloids and Surfaces A: Physicochemical and Engineering Aspects. 2003;220(1-3):261-9.
27. Fu Y-P, Lin C-H. Preparation of CexZr1−xO2 powders by microwave-induced combustion process. Journal of Alloys and Compounds. 2003;354(1-2):232-5.
28. Salavati-Niasari M, Davar F, Mazaheri M. Preparation of ZnO nanoparticles from [bis(acetylacetonato)zinc(II)]–oleylamine complex by thermal decomposition. Materials Letters. 2008;62(12-13):1890-2.
29. Salavati-Niasari M, Davar F. Synthesis of copper and copper(I) oxide nanoparticles by thermal decomposition of a new precursor. Materials Letters. 2009;63(3-4):441-3.
30. Salavati-Niasari M, Davar F, Mazaheri M. Synthesis and characterization of ZnS nanoclusters via hydrothermal processing from [bis(salicylidene)zinc(II)]. Journal of Alloys and Compounds. 2009;470(1-2):502-6.
31. Davar F, Fereshteh Z, Salavati-Niasari M. Nanoparticles Ni and NiO: Synthesis, characterization and magnetic

properties. Journal of Alloys and Compounds. 2009;476(1-2):797-801.
32. Jang Y-I, Wang H, Chiang Y-M. Room-temperature synthesis of monodisperse mixed spinel (CoxMn1−x)3O4 powder by a coprecipitation method. Journal of Materials Chemistry. 1998;8(12):2761-4.
33. Jeong H-M, Kim H-J, Rai P, Yoon J-W, Lee J-H. Cr-doped Co3O4 nanorods as chemiresistor for ultraselective monitoring of methyl benzene. Sensors and Actuators B: Chemical. 2014;201:482-9.
34. Rahman MM, Khan SB, Gruner G, Al-Ghamdi MS, Daous MA, Asiri AM. Chloride ion sensors based on low-dimensional α-MnO2–Co3O4 nanoparticles fabricated glassy carbon electrodes by simple I-V technique. Electrochimica Acta. 2013;103:143-50.
35. Lin C-H, Tsai C-H, Chang H-C. A Convenient Preparation Method for Synthesizing Formamidine Utilizing Sulfated Zirconia. Catalysis Letters. 2005;104(3-4):135-40.
36. Farmer VC. (J. A.) Gadsden. The infrared spectra of minerals and related inorganic compounds. London (Butterworths), 1975. 277 pp. Price £15.00. Mineralogical Magazine. 1976;40(313):540.
37. Ai L-H, Jiang J. Rapid synthesis of nanocrystalline Co3O4 by a microwave-assisted combustion method. Powder Technology. 2009;195(1):11-4.
38. Wen Z, Zhu L, Mei W, Hu L, Li Y, Sun L, et al. Rhombus-shaped Co3O4 nanorod arrays for high-performance gas sensor. Sensors and Actuators B: Chemical. 2013;186:172-9.
39. Wilson AJC. The Powder Method in X-ray Crystallography by L. V. Azaroff and M. J. Buerger. Acta Crystallographica. 1958;11(5):376-.
40. Gu F, Wang SF, Lü MK, Zhou GJ, Xu D, Yuan DR. Structure Evaluation and Highly Enhanced Luminescence of Dy3+-Doped ZnO Nanocrystals by Li+Doping via Combustion Method. Langmuir. 2004;20(9):3528-31.
41. Babakhani B, Ivey DG. Investigation of electrochemical behavior of Mn–Co doped oxide electrodes for electrochemical capacitors. Electrochimica Acta. 2011;56(13):4753-62.
42. Ding Y, Xu L, Chen C, Shen X, Suib SL. Syntheses of Nanostructures of Cobalt Hydrotalcite Like Compounds and Co3O4 via a Microwave-Assisted Reflux Method. The Journal of Physical Chemistry C. 2008;112(22):8177-83.
43. Abu-Zied BM, Soliman SA. Nitrous Oxide Decomposition Over MCO3–Co3O4 (M = Ca, Sr, Ba) Catalysts.Catalysis Letters. 2009;132(3-4):299-310.
44. Ichiyanagi Y, Kimishima Y, Yamada S. Magnetic study on Co3O4 nanoparticles. Journal of Magnetism and Magnetic Materials. 2004;272-276:E1245-E6.
45. Jackson LC, DeWitt C, Dreyfus B, De Gennes PG, Grosewald P. Low Temperature Physics and Low-Temperature Physics. Physics Today. 1963;16(5):68-70.
46. Ambrose T, Chien CL. Finite-Size Effects and Uncompensated Magnetization in Thin Antiferromagnetic CoO Layers. Physical Review Letters. 1996;76(10):1743-6.
47. Kodama RH, Makhlouf SA, Berkowitz AE. Finite Size Effects in Antiferromagnetic NiO Nanoparticles. Physical Review Letters. 1997;79(7):1393-6.
48. Wang Y, Yang CM, Schmidt W, Spliethoff B, Bill E, Schüth F. Weakly Ferromagnetic Ordered Mesoporous Co3O4Synthesized by Nanocasting from Vinyl-Functionalized CubicIa3dMesoporous Silica. Advanced Materials. 2004;17(1):53-6.
49. Salabaş EL, Rumplecker A, Kleitz F, Radu F, SchÃ¼th F. Exchange Anisotropy in Nanocasted Co3O4Nanowires. Nano Letters. 2006;6(12):2977-81.
50. Resnick DA, Gilmore K, Idzerda YU, Klem MT, Allen M, Douglas T, et al. Magnetic properties of Co3O4 nanoparticles mineralized in Listeria innocua Dps. Journal of Applied Physics. 2006;99(8):08Q501.
51. Ye SL, Song WH, Dai JM, Wang KY, Wang SG, Zhang CL, et al. Reply to the "Comment on papers 'Effect of Ag substitution on the transport property and magnetoresistance of LaMnO3' [J. Magn. Magn. Mater. 248 (2002) 26] and 'Possible magnetic phase separation in Ru doped La0.67Ca0.33 [J. Magn. Magn. Mater. 257 (2003) 195]". J Magn Magn Mater. 2004;270(1-2):244-246.
52. Li S, Bi H, Cui B, Zhang F, Du Y, Jiang X, et al. Anomalous magnetic properties in Co3O4 nanoparticles covered with polymer decomposition residues. Journal of Applied Physics. 2004;95(11):7420-2.
53. Farhadi S, Jahanara K, Sepahdar A. Sol–gel derived LaFeO3/SiO2 nanocomposite: synthesis, characterization and its application as a new, green and recoverable heterogeneous catalyst for the efficient acetylation of amines, alcohols and phenols. Journal of the Iranian Chemical Society. 2013;11(4):1103-12.